

**Broadband and Omnidirectional Antireflection Coating based on Semiconductor Nanorods\*\***

By *Silke L. Diedenhofen\**, *Gabriele Vecchi*, *Rienk E. Algra*, *Alex Hartsuiker*, *Otto L. Muskens*, *George Immink*, *Erik P.A.M. Bakkers*, *Willem L. Vos*, and *Jaime Gómez Rivas*

[\*] S. L. Diedenhofen, Dr. G. Vecchi, Dr. J. Gómez Rivas  
FOM Institute for Atomic and Molecular Physics, c/o Philips Research Laboratories,  
High Tech Campus 4, 5656 AE Eindhoven, The Netherlands  
E-mail: [diedenhofen@amolf.nl](mailto:diedenhofen@amolf.nl), <http://www.nanowirephotonics.com>

A. Hartsuiker, Dr. O. L. Muskens  
FOM Institute for Atomic and Molecular Physics, Kruislaan 407,  
1098 SJ Amsterdam, The Netherlands  
Prof. Dr. W. L. Vos

FOM Institute for Atomic and Molecular Physics, Kruislaan 407,  
1098 SJ Amsterdam, The Netherlands  
Complex Photonic Systems, MESA+ Institute for Nanotechnology, University of Twente,  
PO Box 217, 7500 AE Enschede, The Netherlands

Dr. E. P. A. M. Bakkers  
Philips Research Laboratories,  
High Tech Campus 4, 5656 AE Eindhoven, The Netherlands  
R. E. Algra

c/o Philips Research Laboratories,  
High Tech Campus 4, 5656 AE Eindhoven, The Netherlands  
Materials Innovation Institute (M2i), 2628 CD Delft, The Netherlands  
Institute for Molecules and Materials (IMM), Solid State Chemistry Department,  
Radboud University Nijmegen, Toernooiveld 1, 6525 ED Nijmegen, The Netherlands.

[\*\*] We thank E. Evens and W. van den Einden for technical assistance, H. de Barse and F. Holthuysen for SEM analysis, M. A. Verheijen for TEM analysis, H. Jagt for assistance during the measurements, and P. Johnson for useful discussions. This work is part of the research program of the "Stichting voor Fundamenteel Onderzoek der Materie (FOM)", which is financially supported by the "Nederlandse organisatie voor Wetenschappelijk Onderzoek (NWO)" and is part of an industrial partnership program between Philips and FOM. For REA the work was carried out under project number MC3.05243 in the framework of the strategic research program of the Materials Innovation Institute (M2i)

Keywords: Semiconductor Nanorods, Thin Films

Over the last years, there has been an increasing interest in reducing the reflection of surfaces by fabricating antireflection coatings.<sup>[1-16]</sup> Antireflection coatings can be applied to minimize the reflection for optical components,<sup>[4]</sup> to improve the light coupling into solar cells<sup>[5]</sup> or to enhance the extraction of light from LED's.<sup>[6]</sup> Depending on the structure of the antireflection

layers, these can be classified into two types: (i) antireflection coatings made of homogeneous layers and (ii) formed by inhomogeneous layers.<sup>[15]</sup> Homogeneous antireflection coatings, or step index coatings, reduce the reflection by destructive interference of light reflected at different interfaces. For these coatings the material and thickness of the layer have to be chosen carefully for each wavelength, angle, and substrate. The bandwidth of these coatings is lower than one octave, e.g. 400 nm to 700 nm or 800 nm to 1100 nm, and the angle of incidence is limited to 30 °.<sup>[16]</sup> The other type of antireflection coatings, or the inhomogeneous layers, form the so-called graded index coatings. They are advantageous over step index coatings with respect to omnidirectionality and broadband behavior. Theoretically, a drastic reduction of the reflection for angles up to 80 ° and for a wavelength range of one order of magnitude is shown, e.g. 400 nm to 4 μm.<sup>[3]</sup> In this kind of coating, the refractive index is gradually increased from that of the surrounding material to the refractive index of the substrate and the reflection is decreased by optical impedance matching at the interfaces. **Figure 1a** shows a schematic representation of the reflection of a substrate with a homogeneous and with a graded index coating.

The fabrication of graded index coatings is very challenging when the substrate is surrounded by air, as a solid material is needed which matches a refractive index of 1. Obviously, the refractive index of any dense solid material is too large to match the refractive index of air. To overcome this problem, more effort has been made over the last years to obtain graded index coatings by applying nanostructuring techniques inspired by biological structures like moth-eyes.<sup>[17,18]</sup> With these techniques, it is possible to fabricate layers of porous materials which have an effective refractive index close to 1 on the upper part and a larger index at the bottom. Recently, a graded refractive index structure has been fabricated in a bottom-up process using SiO<sub>2</sub> and TiO<sub>2</sub> nanorods deposited on AlN.<sup>[7]</sup> Using this technique, a graded index is achieved by varying the filling fraction from one layer to the next and by changing the material from a low index material at the top (SiO<sub>2</sub>) to a material with a higher refractive index at the bottom

(TiO<sub>2</sub>). Therefore, for these coatings the evaporation of two materials is necessary. A different bottom-up approach based on chemical vapor deposition has led to recent demonstrations of antireflection coatings consisting of single materials.<sup>[5]</sup> These coatings are formed by ZnO nanowires grown on a Si substrate. The use of silicon substrates in Ref. [5] did not allow transmission measurements for visible wavelengths, and the effects of light scattering by the nanowires on the reduction of the reflection could not be determined. With top-down nanostructuring processes, the reflection of Si has been reduced by etching different kinds of nanostructures into the substrate.<sup>[8-11]</sup> With these etching techniques, very low values of the zeroth-order or specular reflection have been reported. However, it has not been clearly stated whether this reduced reflection occurs due to light scattering by the nanostructures, to an enhanced absorption in the antireflection layer, to refractive index matching to the substrate, or to a combination of these phenomena. An important limitation of etched silicon surfaces is that the antireflection layer is also absorbing. The fabrication of non-absorbing antireflection layers on top of absorbing substrates is thus impossible by etching. It is also worth mentioning the ultralow reflection recently reported in layers of carbon nanotubes.<sup>[12,13]</sup> This reduced reflection was mainly caused by absorption.

Here, we unambiguously demonstrate by measuring the transmission and reflection of GaP nanorods on top of a GaP substrate, that the reduction of the reflection in these layers is mainly caused by a graded refractive index coating and interference in the nanorod film and that the role of scattering losses and absorption by the nanorod layer is secondary. The broadband reduction of the reflection is demonstrated by zeroth-order or direct transmission and specular reflection measurements at wavelengths in the visible and near infrared and by angle-integrated total reflection and transmission measurements. To investigate the omnidirectionality of the antireflection coating, transmission and reflection measurements are performed for angles up to 60 °. We have chosen to work with GaP nanorods on top of a GaP substrate, as the electronic band gap of GaP is located at 548 nm, so transmission

measurements are possible for the red and near-infrared part of the spectrum. The investigated coatings of nanorods were fabricated in a bottom-up process using the vapor-liquid-solid (VLS) growth mode<sup>[19]</sup> by chemical vapor deposition. In contrast to etching techniques, this technique allows the heteroepitaxial growth of several semiconductors of groups IV,<sup>[20,21]</sup> III/V,<sup>[22,23]</sup> and II/VI<sup>[5,24]</sup> on different substrates.<sup>[25]</sup>

We have investigated the antireflection properties of two types of nanorods, cylindrically and conically shaped rods. In ensembles of conically shaped nanorods a graded refractive index can be achieved, with a low effective refractive index at the top and a high effective index at the bottom, due to the variation of the filling fraction of GaP along the growth direction of the rods. The cylindrical nanorods show an antireflection behavior due to a distribution of nanorod lengths which leads to a reduced density towards the top of the layer. The investigated coatings of nanorods were fabricated on a double side polished GaP substrate with a thickness of 500  $\mu\text{m}$ . On the backside of the substrate a film of  $\text{SiO}_2$  with a thickness of 500 nm was deposited to avoid etching of this surface during a surface cleaning process before the growth. A more detailed description of the fabrication is given in the experimental section. The growth can be controlled by adjusting the temperature of the substrate during growth in such a way that either vertically aligned cylindrical nanorods or conically shaped nanorods can be fabricated. The initial diameter of the nanorods is determined by the size of gold particles used to catalyze the growth, and thus determines the diameter at the top of the rod. During the vertical growth of the nanorods, it is also possible to induce a side-wall growth when the temperature exceeds the critical value.<sup>[26]</sup> For one of the investigated samples, which will be called sample I, the temperature was such that lateral growth is significant. Since the base of the nanorods is exposed to the side-wall growth for the longest time, the diameter is the largest at this position and it gradually decreases towards the top of the rod. The apex angle of the conical shape can be tuned as at higher temperatures the lateral growth is more pronounced with respect to the vertical growth.<sup>[26]</sup> The other sample, that will

be called sample II, is grown at a lower temperature, where vertical growth is dominating, leading to non-tapered vertically aligned rods.

**Figure 1b** and **Figure 1e** show scanning electron microscopy (SEM) images of samples I and II, respectively. The GaP filling fraction increases from the top to the bottom of the nanorod layer due to tapering for sample I. For sample II an increase in GaP filling fraction occurs because of the nanorod length distribution. **Figure 1c** and **Figure 1f** show top-view SEM images of samples I and II, respectively. The density of nanorods for sample II is higher than for sample I, while the nanorods in sample I have a larger diameter at the bottom. The difference in density is due to different growth conditions for both samples (see experimental section). As has been observed before and we have confirmed with sample II, variations in rod density and diameter lead to a distribution in the length of the rods.<sup>[22]</sup> A histogram representing the length distribution of sample II is given in **Figure 1d**. This distribution is obtained by measuring the length of 56 nanorods from SEM images like Figure 1e. The length of the rods varies from 50 nm up to 250 nm, while the majority of rods have a length of 250 nm. The growth parameters and the characteristic dimensions for both samples are summarized in **Table 1**. To further verify the structure of the nanorods, **Figure 2a** and **2b** show transmission electron microscopy (TEM) images of both type of rods. On all rods, the gold particle on top is visible. The darker and lighter regions of the rods are related to twinning defects.<sup>[27]</sup> These defects do not have an significant effect on the nanorod refractive index and do not modify reflection characteristics of an nanorod layer.<sup>[27,28]</sup> These images show a clear difference between the conically shaped (Figure 2a) and cylindrical rods (Figure 2b). For the conical rods, a tapering angle of around 3 ° can be estimated.

We have determined the broadband specular reflection on and direct transmission through the samples using the setup explained in the experimental section. The transmission was measured at normal incidence while the reflection was measured at an angle of incidence of 6 ° with respect to the surface normal. The resulting transmission and reflection spectra are

displayed in **Figure 3a** and **Figure 3c**, respectively, with light grey circles for sample I and dark grey triangles for sample II. For comparison, we also plot the transmission and reflection measurements of a bare GaP substrate with 500 nm SiO<sub>2</sub> at the backside (black squares). The sharp absorption edge visible for all samples at 2.26 eV ( $\lambda = 548$  nm) is due to the electronic band gap of GaP. The small dip in the transmission and the maximum in the reflection of the GaP substrate around 1.76 eV ( $\lambda = 700$  nm) are due to a Fabry-Pérot resonance in the SiO<sub>2</sub> layer at the backside of the GaP substrate. The scattering losses of the samples can be estimated by adding the transmission and reflection measurements (see **Figure 3e**). For the GaP substrate (black squares), the transmission plus reflection is 100 % for energies below 2.26 eV; as expected, there are no losses in the measurement of the reference below the band gap in GaP. For higher energies, interband absorption has a dominant influence. For sample I, the transmission from around 1.88 eV ( $\lambda = 660$  nm) to 2.3 eV (550 nm), is not increased with respect to the transmission of the bare GaP substrate. At these energies, Rayleigh scattering by the nanorods reduces slightly the transmission of sample I cancelling the enhancement of this transmission due to the antireflection.<sup>[27]</sup> For lower energies, however, the transmission increases as scattering losses become negligible. At 1.38 eV ( $\lambda = 900$  nm), the transmission of sample I is increased by 20 % compared to the substrate. The small shift of the dip in transmission and the peak in reflection at around 1.85 eV (670 nm) compared to the transmission and reflection of the substrate is related to a Fabry-Pérot reflection in the nanorod layer superimposed to the reflection in the back SiO<sub>2</sub> layer. The sum of reflection and transmission (Figure 3e) for sample I (light grey circles) increases from 85 % at 2.15 eV ( $\lambda = 575$  nm) to around 95 % at 1.38 eV ( $\lambda = 900$  nm). The small reduction of the sum of reflection and transmission when increasing the energy can be attributed to light scattering in the nanorod layer.

From the transmission measurement of sample II (dark grey triangles in Figure 3a), we can estimate an increase of the transmission of around 13 % relative to the bare GaP substrate for energies below the electronic band gap. This nanorod antireflection coating consists of thinner nanorods than sample I (see Table 1), so Rayleigh scattering is less pronounced in the range of wavelengths considered. For this sample, the sum of reflection and transmission (dark grey triangles in Figure 3e) shows a flat wavelength response of around 95 %. The slightly lower than 100% measured sum of reflection and transmission can be assigned to residual scattering in the nanorod layer and surface roughness due to the length distribution of the wires.

Importantly, the enhanced transmission measurements of Figure 3a demonstrates that the reduction in specular reflection reported in Figure 3c is not only due to surface roughness or scattering in the nanorod layer, but also to the refractive index matching that the nanorod layer provides between air and GaP.

**Figure 3b, 3d, and 3f** show calculations of the transmission and reflection, performed using the thin-film method,<sup>[29]</sup> of sample I (light grey dash dot dotted curve), sample II (dark grey dashed curve) and a bare GaP substrate covered on one side with a 500 nm thick SiO<sub>2</sub> layer (black solid curve). The calculated system consists of 5 layers: air, nanorod layer, GaP substrate, SiO<sub>2</sub>, and air. The nanorod layer is considered as sliced into 50 horizontal sub-layers, each of which has a thickness of 5 nm. We assume for sample I that the refractive index per sub-layer increases quadratically with the length of the nanorods. This quadratic increase is based on the assumption that the filling fraction is proportional to the square of the diameter of the rods and that the effective refractive index is proportional to the GaP filling fraction. From the calculations, we have determined a variation of the refractive index over the nanorod layer length of sample I from 1.1 up to 2.1. The length distribution of the rods of sample II is determined from SEM images (Figure 1e). From this length distribution we can estimate a refractive index profile which results in a third-order polynomial as a function of depth, in which the refractive index is varied from 1.1 to 1.4 over the nanorod layer length.

The calculations (Figure 3b, d, f) show the same trend as the measurements (Figure 3a, c, e).

The small discrepancies with the measurement can be attributed to the aforementioned scattering, which is not included in the calculations. Both measurement and calculation show a reduction for the sum of transmission and reflection (Figure 3e and f) with respect to the bare GaP substrate for energies higher than the electronic band gap of GaP. This reduction can be attributed to scattering of light and to an enhanced absorption in GaP due to the antireflection coating. From calculations performed assuming the nanorod layers positioned on top of an infinite thick GaP substrate (not shown here), we have established that the modulation of the transmission and reflection through samples I and II are due to Fabry-Pérot resonances in the SiO<sub>2</sub> layer at the bottom of the wafer and at the nanorod film on top. This indicates that the nanorod layer acts both as a graded refractive index coating and a single layer interference coating.

In addition to direct transmission and specular reflection measurements, we have performed angle-integrated total reflection and transmission measurements for energies between 0.62 eV ( $\lambda = 2000$  nm) and 2.58 eV ( $\lambda = 480$  nm) as described in the experimental section. For these measurements both the specular or direct light beam and the possibly scattered light are collected using an integrating sphere. **Figure 4a** shows the total transmission of sample I (light grey circles) and II (dark grey triangles) for normal incidence, while **Figure 4b** displays the total reflection measurement of both samples for an angle of incidence of 8 ° with respect to the normal of the sample. These total transmission and reflection spectra have been normalized by reference measurements of a GaP substrate. The total transmission measurement shows for energies below the electronic band gap and for both samples an increase with respect to bulk GaP. The overall reduction of the total reflection with respect to the substrate (Figure 4b) demonstrates that the reduction of the specular reflection of Figure 3c is not due to light scattering in the nanorod film: if the reduction of the specular reflection had been caused by scattering, the angle-integrated total reflection measurement would not

show a decreased reflection with respect to the GaP reference, as both scattered light and specular reflection are detected. The dip in normalized reflection at around 1.35 eV ( $\lambda = 900$  nm) is caused by the aforementioned combination of a Fabry-Pérot oscillation in the SiO<sub>2</sub> layer at the backside of the GaP substrate and in the nanorod film. As can be seen in Figure 4c, the sum of total transmission and total reflection with respect to the bare GaP substrate is 1 for energies less than 2.26 eV, which shows that there are no absorption losses at these energies. Above the electronic band gap of GaP, there is a reduction of the total transmission plus reflection of the nanorod layer with respect to the bare GaP substrate (see **Figure 4c**). This reduction means an enhanced absorption in the nanorod antireflection coating. In summary, these measurements show that layers of nanorods form broadband antireflection coatings which reduce the total reflection and enhance the total transmission from 2.25 eV ( $\lambda = 550$  nm) to at least 0.62 eV ( $\lambda = 2000$  nm).

To investigate the omnidirectional characteristics of these antireflection coatings, we have performed direct transmission and specular reflection measurements as a function of wavelength in the range from 550 nm to 900 nm and for angles of incidence varying from 0 ° to 60 ° for sample II. This angular range was limited by our experimental setup. **Figure 5a** shows a contour image of the transmission of the nanorod sample normalized to the transmission of the GaP substrate. For all wavelengths and at all angles a transmission exceeding 1 is observed. **Figure 5b** shows the angle dependent transmission for a wavelength of 750 nm taken along the black dotted line in Figure 5a. **Figure 5c** and **Figure 5d** show the reflection of sample II normalized to the reflection of the GaP reference. The normalized reflection is less than 1 for all wavelengths and in the investigated angular range. Based on these measurements, we conclude that the nanorod layers act as broadband and omnidirectional antireflection coatings.

In summary, we have investigated the antireflective properties of layers of GaP nanorods using wavelength and angle dependent transmission and reflection measurements. The

nanorods were fabricated by chemical vapor deposition using the vapor-liquid-solid method.

We have shown that the enhanced transmission and corresponding reduced reflection of these layers is related to a graded refractive index in the nanorod layer. The enhanced direct transmission and the total transmission and reflection presented in this article show that scattering and absorption are weak in these layers. The antireflection behavior over a broad wavelength and angular range and the low amount of light scattering makes these nanorod antireflection coatings a very promising material for enhancing light coupling in solar cells or for more efficient light extraction of LED's.

### *Experimental*

*Growth of Nanorods:* Before growth, the (111)A (Ga-terminated) side of the GaP substrate was covered with 500 nm of SiO<sub>2</sub> by plasma enhanced chemical vapor deposition at a temperature of 300 °C to protect the backside during the anisotropic etching of the wafer in HNO<sub>3</sub>:HCl:H<sub>2</sub>O (2:3:3) at 80 °C for 2 min. This etching step is necessary to remove any native oxides which would hinder the nanorod growth. Directly after etching, a thin gold film with a thickness of 0.3 nm was deposited onto the (111)B GaP (P-terminated) substrate side. This gold film acts as a catalyst for the nanorod growth. During annealing the gold film breaks up into small islands, which form individual catalyst droplets from which the nanorods grow selectively. The gold film of sample I was annealed for 10 minutes at 570 °C, for sample II this step was left out. The nanorods are grown in the vapor-liquid-solid-growth mode in a low-pressure (50 mbar) metal-organic vapor phase epitaxy system (Aixtron 200) using trimethylgallium (TMG) and phosphine (PH<sub>3</sub>) as precursors, with molar fractions of  $\chi_{\text{TMG}} = 9.1 \cdot 10^{-5}$  and  $\chi_{\text{PH}_3} = 15 \cdot 10^{-3}$ . A total flow of 6 l/min was used, with hydrogen (H<sub>2</sub>) as carrier gas. After growth, the samples were cooled down in a PH<sub>3</sub> containing atmosphere.

*Angle-resolved specular reflection and direct transmission measurements:* We performed wavelength and angle dependent transmission and reflection measurements for wavelengths between 1.38 eV ( $\lambda = 900$  nm) and 2.58 eV ( $\lambda = 480$  nm) by mounting the sample and

detector on a set of computer controlled rotation stages. The samples were illuminated using a collimated beam of a fiber-coupled halogen lamp (Yokogawa AQ4303) and the spectra were obtained using a spectrometer (Ocean Optics, USB2000).

*Angle-integrated total reflection and transmission measurements:* This measurement was performed using a Lambda 950 spectrometer (Perkin Elmer) consisting of a tungsten-halogen and a deuterium lamp and an integrating sphere in combination with a photomultiplier for the visible and a PbS detector for infrared light. For the transmission measurement, the samples were mounted in front of the integrating sphere, so that all the transmitted light was collected. For the reflection measurement, the samples were mounted at the backside of the integrating sphere with an angle of  $8^\circ$  with respect to the incident light beam, so that all the reflected light from the sample could be collected and detected.

Received: ((will be filled in by the editorial staff))

Revised: ((will be filled in by the editorial staff))

Published online: ((will be filled in by the editorial staff))

- \_ [1] W. H. Southwell, *Opt. Lett.*, **1983**, 8, 584
- \_ [2] J. A. Dobrowolski, D. Poitras, P. Ma, H. Vakil, M. Acree, *Appl. Opt.*, **2002**, 41, 3075
- \_ [3] D. Poitras, J. A. Dobrowolski, *Appl. Opt.*, **2004**, 43, 1286
- \_ [4] T. Lohmüller, M. Helgert, M. Sundermann, R. Brunner, and J. P. Spatz, *Nano Lett.*, **2008**, 8, 1429
- \_ [5] Y.-J. Lee, D. S. Ruby, D. W. Peters, B. B. McKenzie, and J. W. P. Hsu, *Nano Lett.*, **2008**, 8, 1501
- \_ [6] S. J. An, J. H. Chae, G.-C. Yi, and G. H. Park, *Appl. Phys. Lett.*, **2008**, 92, 121108
- \_ [7] J.-Q. Xi, M. F. Schubert, J. K. Kim, E. F. Schubert, M. Chen, S.-Y. Lin, W. Liu, and J. A. Smart, *Nature Photonics*, **2007**, 1, 178

- \_[8] Y.-F. Huang, S. Chattopadhyay, Y.-J. Jen, C.-Y. Peng, T.-A. Liu, Y.-K. Hsu, C.-L. Pan, H.-C. Lo, C.-H. Hsu, Y.-H. Chang, C.-S. Lee, K.-H. Chen, L.-C. Chen, *Nature Nanotechnol.*, **2007**, 2, 770
- \_[9] C. H. Sun, W.-L. Min, N. C. Linn, P. Jiang, and B. Jiang, *Appl. Phys. Lett.*, **2007**, 91, 231105
- \_[10] C. H. Sun, P. Jiang, and B. Jiang, *Appl. Phys. Lett.*, **2008**, 92, 061112
- \_[11] Z. Yu, H. Gao, W. Wu, H. Ge, and S. Y. Ghou, *J. Vac. Sci. Technol. B*, **2003**, 21, 2874
- \_[12] Z. P. Yang, L. C. Ci, J. A. Bur, S. Y. Lin, and P. M. Ajayan, *Nano Lett.*, **2008**, 8, 446
- \_[13] F. J. Garcia-Vidal, *Nature Photonics*, **2008**, 2, 215
- \_[14] C. H. Chiu, P. Yu, H. C. Kuo, C. C. Chen, T. C. Lu, S. C. Wang, S. H. Hsu, Y. J. Cheng, and Y. C. Chang, *Optics Express*, **2008**, 16, 12, 8748
- \_[15] J. A. Dobrowolski in *Handbook of Optics*, Vol. 1 (Eds: M. Bass, E. W. van Stryland, D. R. Williams, W. L. Wolfe), McGraw-Hill, Inc., New York, **1995**, Ch. 42
- \_[16] D. S. Hobbs, B. D. Macleod, and J. R. Riccobono, *Proc. SPIE*, **2007**, 6545, 65450y
- \_[17] C. G. Bernhard, *ENDEAVOUR*, **1967**, 26, 79
- \_[18] D. G. Stavenga, S. Foletti, G. Palasantzas, and K. Arikawa, *Proc. R. Soc. B*, **2006**, 273, 661
- \_[19] R.S. Wagner and W.C. Ellis, *Appl. Phys. Lett* , **1964**, 4, 89
- \_[20] L. J. Lauhon, M. S. Gudixsen, D. Wang, C. M. Lieber, *Nature*, **2002**, 420, 57
- \_[21] J. B. Hannon, S. Kodambaka, F. M. Ross, R. M. Tromp, *Nature*, **2006**, 440, 69
- \_[22] M.T.Borgström, G. Immink, B. Ketelaars, R. Algra and E.P.A.M Bakkers, *Nature Nanotechnol.*, **2007**, 2, 541
- \_[23] M. T. Björk, B. J. Ohlsson, T. Sass, A. I. Persson, C. Thelander, M. H. Magnusson, K. Deppert, L. R. Wallenberg, and L. Samuelson, *Nano Lett.*, **2002**, 2, 87
- \_[24] M. H. Huang, S. Mao, H. Feick, H. Yan, Y. Wu, H. Kind, E. Weber, R. Russo, P. Yang, *Science*, **2001**, 292, 1897

\_[25] K. Hiruma, M. Yazawa, T. Katsuyama, K. Ogawa, K. Haraguchi, M. Koguchi, and H. Kakibayashi, *J. Appl. Phys.*, **1995**, 77, 447

\_[26] M.A. Verheijen, G. Immink, T. de Smet, M.T. Borgström and E.P.A.M. Bakkers, *J. Am. Chem. Soc.*, **2006**, 128, 1353.

\_[27] O. L. Muskens, S. L. Diedenhofen, M. H. M. Van Weert, M. T. Borgström, E. P. A. M. Bakkers, and J. Gómez Rivas, *Adv. Funct. Mater.*, **2008**, 18, 7, 1039

\_[28] O. L. Muskens, M. T. Borgström, E. P. A. M. Bakkers, and J. Gómez Rivas, *Appl. Phys. Lett.*, **2006**, 89, 233117

\_[29] P. Yeh, *Optical Waves in Layered Media*, John Wiley & Sons, New York, Chichester, Brisbane, Toronto, Singapore, **1948**, Ch. 6

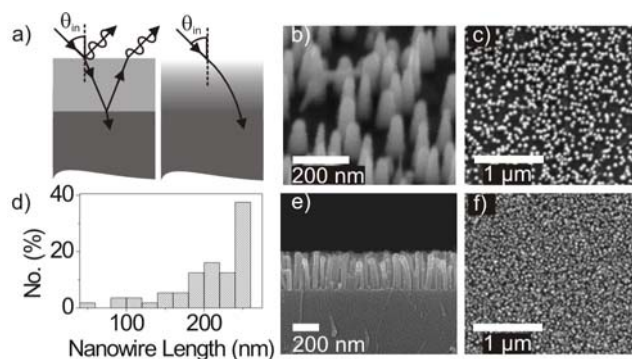


**Figure 1.** a) Schematic of the reflections of a substrate with a homogeneous (left) and with a graded refractive index coating (right). The homogeneous coating reduces the reflection due to interference of light reflected at the air-coating layer and at the coating layer-substrate interfaces. For simplicity, just one reflection path is shown which stands for the multiple reflections occurring at the interfaces. For the graded index coating, no reflection occurs as the refractive index is matched at the top and bottom interfaces. b,c,e,f) Scanning electron images of nanorods. b) Image of conically shaped nanorods (sample I) tilted under  $30^\circ$  with respect to the normal of the sample. c) Top-view image of the same sample e) Side-view image of cylindrical nanorods (sample II). f) Top-view image of the same sample. The SEM image in b) is magnified to show the tapering of the wires, the image in e) shows more

nanorods to display the distribution in length of the rods. d) Distribution of the length of the nanorods of sample II.

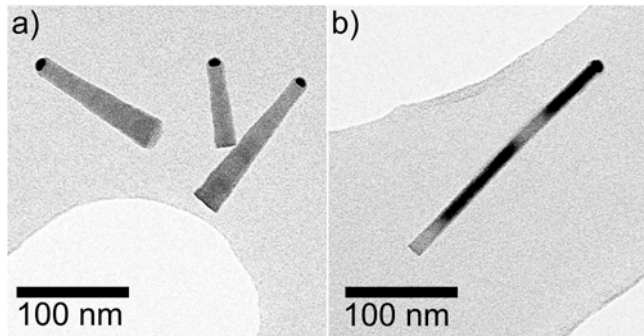
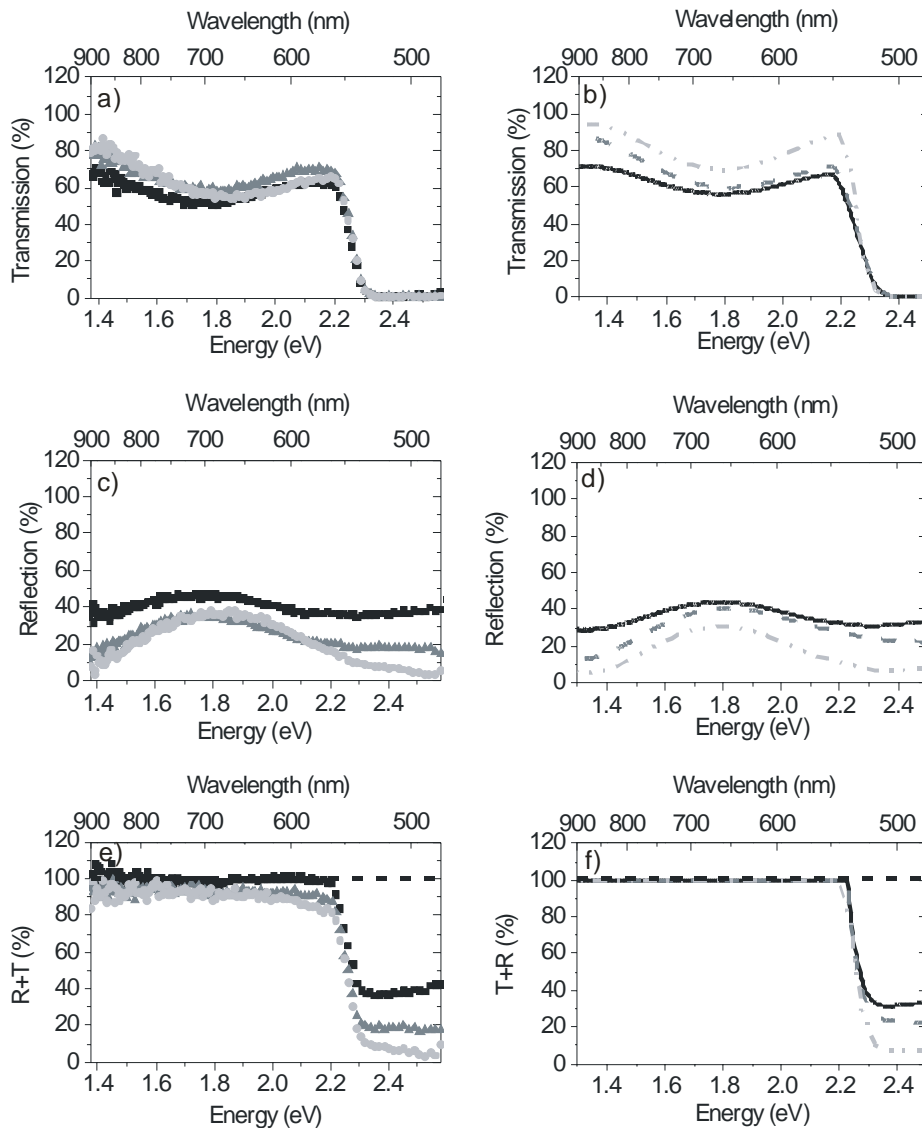
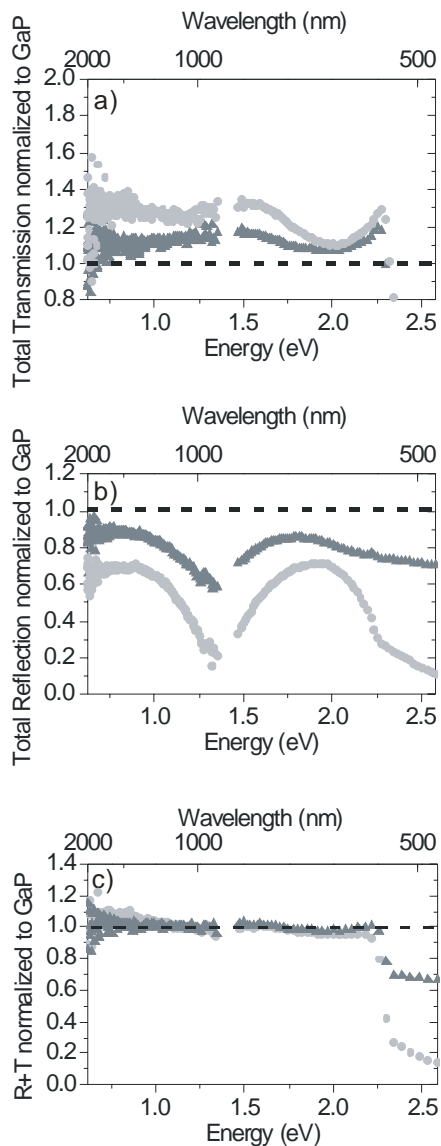


Figure 2. Transmission electron microscopy images of a) conical nanorods (sample I) and b) cylindrical nanorods.



**Figure 3.** a) Measured transmission for normal incidence, c) measured reflection at an angle of incidence of  $6^\circ$  and e) the sum of measured reflection and transmission. b) Calculated transmission for normal incidence, d) calculated reflection at an angle of incidence of  $6^\circ$  and f) the sum calculated of reflection and transmission. The measurements (calculations) for a bare GaP substrate with one side covered by a layer of 500 nm of SiO<sub>2</sub> are the black squares (black solid curve). The light grey circles (light grey dash dot dotted curve) and the dark grey triangles (dark grey dashed curve) correspond to the measurements (calculations) of sample I and II, respectively.



**Figure 4.** Total transmission a) and total reflection b) of sample I (light grey circles) and II (dark grey triangles) normalized to the measurements on a GaP substrate. c) Sums of the total

reflection and transmission of samples I (light grey circles) and II (dark grey triangles)

normalized to the total reflection and transmission of the bare GaP substrate.

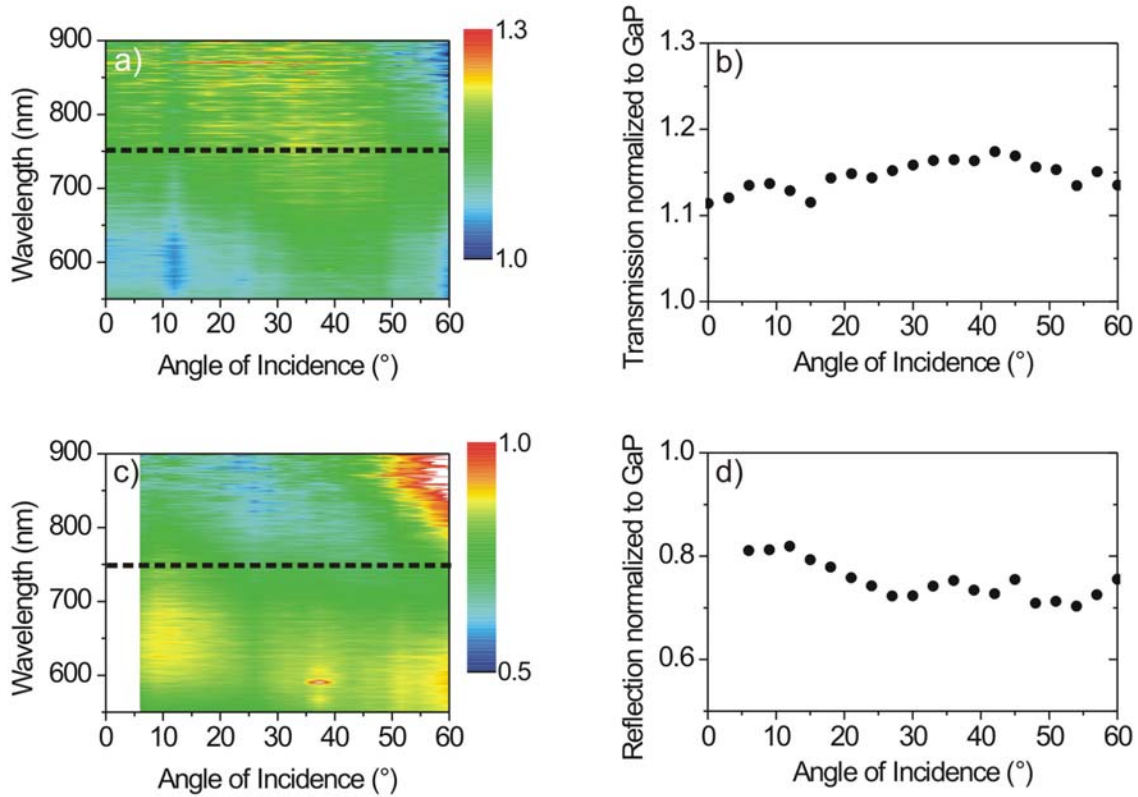


**Figure 5.** a) Angular dependent transmission and c) reflection of a layer of GaP nanorods of sample II normalized to the transmission and reflection of a bare GaP substrate. b) and d) show the transmission and reflection measurements at 750 nm (along the dotted lines of a) and c)).

**Table 1.** Growth time and temperature of GaP nanorods. Sample I consists of conically shaped nanorods, while sample II is formed by cylindrical structures. The averaged nanorod length and diameter at the top and bottom part of the nanorods are also listed. These values are obtained from SEM images.

Sample	Growth time [s]	Growth temperature [°C]	Length [nm]	Top diameter [nm]	Bottom diameter [nm]
I	600	570	178 ± 25	28 ± 7	63 ± 9
II	320	420	208 ± 50	27 ± 5	27 ± 5

Table of Contents entry:

**A broadband and omnidirectional antireflection coating** consisting of semiconductor nanowires is fabricated. The reflection is reduced due to a graded refractive index that is achieved by a certain nanorod length distribution of cylindrical nanorods and by conically shaped rods. By means of a systematic optical investigation, combining transmission and reflection measurements, an increased transmission and accordingly a reduced reflection is demonstrated for the visible and near infrared part of the spectrum.

Keyword (see list): Semiconductor Nanorods, Thin Films

Silke L. Diedenhofen\*, Gabriele Vecchi, Rienk E. Algra, Alex Hartsuiker, Otto L. Muskens, George Immink, Erik P.A.M. Bakkers, Willem L. Vos, and Jaime Gómez Rivas

Broadband and Omnidirectional Antireflection Coating based on Semiconductor Nanorods

ToC figure

